Title

THE DEVELOPMENT OF A FERRITIC CONSUMABLE FOR WELDING GRAIN-REFINED Fe-12Ni-0.25Ti TO RETAIN TOUGHNESS AT 4.2K

Author

Morris, J.W.

Publication Date

1981-08-01

LBL-13046
Preprint

Lawrence Berkeley Laboratory
UNIVERSITY OF CALIFORNIA

Materials & Molecular
Research Division

Submitted to Welding Journal

THE DEVELOPMENT OF A FERRITIC CONSUMABLE FOR WELDING GRAIN-REFINED Fe-12Ni-O.25Ti TO RETAIN TOUGHNESS AT 4.2K

H.J. Kim and J.W. Morris, Jr.

August 1981

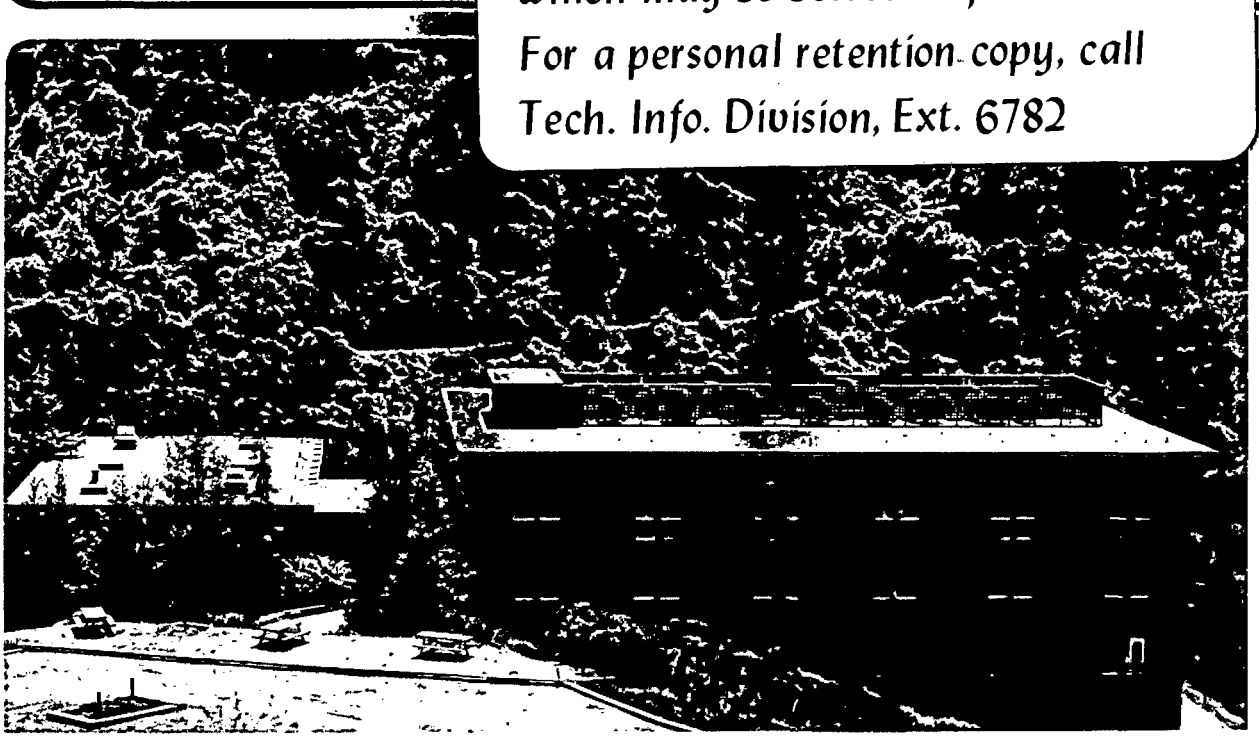

Prepared for the U.S. Department of Energy under Contract W-7405-ENG-48

DISCLAIMER

LBL-13046

THE DEVELOPMENT OF A FERRITIC CONSUMABLE FOR WELDING GRAIN-REFINED Fe-12Ni-0.25Ti TO RETAIN TOUGHNESS AT 4.2K

By

H. J. Kim and J. W. Morris, Jr.

Materials and Molecular Research Division
Lawrence Berkeley Laboratory

and

Department of Materials Science
and
Mineral Engineering

University of California, Berkeley, CA. 94720

This work was supported by the Director, Office of Energy Research, Office of Development and Technology, Magnetic Systems Division of the U.S. Department of Energy under Contract Number W-7405-ENG-48.

ABSTRACT

A multi-pass gas tungsten arc welding (GTAW) process has been developed for welding grain-refined Fe-12Ni-0.25Ti steel with a matching ferritic 14% filler metal. The weldment is deposited as multi-pass weldment in a single V joint at heat inputs from 7-17 kJ/cm. The ferritic weldment has a strength roughly matching that of the base plate, and exhibits excellent toughness both in the weld metal and in the heat-affected zone at temperatures as low as liquid helium temperature (4.2K). The excellent toughness is attributed to two factors: the chemical cleanliness of the GTAW deposit, and the refined microstructure of the weldment and the retention of fine microstructure in the heat-affected zone. The grain refinement is accomplished by the sequential rapid thermal cycles experienced by the material during multi-pass GTAW welding.

INTRODUCTION

Previous research (1-3) in this laboratory has demonstrated that the ductile-brittle transition temperature of Fe-(9-12)%Ni ferritic cryogenic steels can be suppressed to below 4.2K by applying heat treatments which establish an ultra-fine effective grain size. In particular, a laboratory Fe-12Ni-0.25Ti alloy has been grain-refined by a four-step (2B) thermal cycling treatment and a commercial Fe-9Ni alloy has been processed through a five-step (2BT) treatment to achieve excellent combinations of strength and toughness at 4.2K. These alloys have potential applications in the structures of high field superconducting magnets. Since the structures of such magnets are almost invariably welded, their applicability requires the development of weld wire chemistries and welding procedures which preserve good 4K properties.

The welding problem is, at least superficially, a formidable one. The good cryogenic properties of the base alloys are achieved through the use of heat treatments which establish a rather precise control over the alloy microstructure. Subsequent welding introduces the simultaneous problems of establishing a suitable microstructure in the weld deposit and retaining an appropriate microstructure in the heat-affected zone.

Initial research on the welding of this (4) and similar alloys (5) for 4K service employed high-nickel Inconel filler metals to avoid the problem of brittleness in the weld deposit. However, the GMA welding of Fe-12Ni-0.25Ti with Inconel 92 filler (4) was partly successful. The Inconel 92 filler was inferior to the ferritic base metal over the whole temperature range, not only in its yield strength but also in its notch toughness. In addition the Inconel 92 weldment exhibited a fusion zone

brittleness which is familiar from other research (6) on the welding of Fe-9%Ni steel with non-matching austenitic fillers; cracks starting in the heat-affected zone tend to propagate along the fusion line.

Recently, however, researchers at Nippon Kokan K.K. and Kobe steel (7) have jointly developed an automatic GTAW process which uses a matching ferritic filler wire to weld quench and tempered 9Ni steel for service at 77K. The success of this procedure is largely due to two advantages of the multi-pass GTAW welding process: the low level of air contamination in the weld deposit and the cyclic heat treatment of the weld deposit by subsequent passes, which is at least partly controllable through independent variation of the heat input and wire feed rate. It is, as a result, possible to obtain a ferritic weld deposit which is both clean and relatively fine-grained and which, consequently, has good toughness at 77K. Preliminary work at the NASA Lewis Research Laboratory (8) suggests that Fe-12Ni-0.25Ti may also be GTAW welded with matching filler for 77K service.

The microstructural constraints which must be satisfied to achieve good toughness at 4K are much more stringent than those required for toughness at 77K. Nonetheless, the metallurgical approach of the multi-pass GTAW process as a means of controlling the microstructure of weldments together with the success which has already been achieved at 77K suggest that this process may be successful for joining ferritic cryogenic steels for 4K service. In the following, we report some very promising initial results of research on the multi-pass GTA welding of Fe-12Ni-0.25Ti steel with matching ferritic filler.

ALLOY PREPARATION AND EXPERIMENTAL PROCEDURE

I. Alloy Preparation.

The compositions of the base alloy and weld filler metals used in this research are given in Table I. The base alloy has a nominal composition, in

weight percent, of Fe-12Ni-0.25Ti. The two filler metals (A and B) have a slightly higher nickel content (14 wt.%) plus intentional additions of other alloying elements. The increase in nickel content was made in the hope of lowering the ductile-brittle transition temperature of the weld metal (9,10). Boron was added to filler metal B in the expectation that it would act as a grain boundary surfactant to promote grain refinement and inhibiit intergranular or intercellular fracture (11,12). The Mn and Si additions to filler metal A were made to expolore their effect on mechanical properties since these are common additions in commercial heats.

Both the base plates and weld filler alloys were cast in this laboratory after vacuum-induction melting from pure starting materials. The base alloy was cast as a 25 lb (9.425 kg) ingot, homogenized at 1200°C for 24 hours under inert atmosphere, and then upset cross-forged at 1100°C into plates of 7 in width and 0.6 in thickness (178 x 15 mm). Each plate was then cut in half and heat treated through the "2B" thermal-cycling treatment diagrammed in Fig. 1. This treatment, which has been described elsewhere (1), establishes a fine microstructure of nearly equiaxed grains of ~1 μm mean diameter. The plates were then machined into the joint configurations described below.

The weld filler metal was cast into 5 lb (9.25 kg) 1 in (25 mm) diameter ingots. After homogenization at 1200°C for 24 hours the ingots were hot rolled into 5/16 in (7.9 mm) square bars at a starting temperature of 1100°C, then hot-swaged to 1/2 in (6.4 mm) diameter round bars and surface ground to remove any oxides. The ground bars were cold-swaged to 1/16 or 3/32 in (1.59 or 2.38 mm) diameter bars, which were used as the filler rod for the manual GTA welding process.

II. Thermal Cycling Studies.

Thermal cycling studies were conducted to gain insight into the response of the alloy to the rapid heating and cooling cycles encountered during welding. All thermal cycling studies were done on the base alloy, Fe-12Ni-0.25Ti, in one of the two starting conditions: the as-annealed condition, which was used as a crude representation of the initial condition of the weld deposit and the "2B" condition, which represented the initial state of the heat-affected zone.

The thermal cycles were imposed on slightly oversized Charpy impact specimens in an induction furnace. The sample was suspended in the center of a 38 mm diameter quartz tube surrounded by the induction coil. For cycles having a peak temperature lower than 1200°C, the temperature was monitored by a chromel-alumel thermocouple connected both to a chart recorder and to a digital indicator. For cycles having peak temperature higher than 1200°C, an optical pyrometer was used. Once the selected peak temperature had been reached the sample was dropped into a quenching bath of either water or oil. An example temperature-time profile for a 1300°C peak temperature cycle with an oil quench is sketched in Fig. 2.

III. Welding Procedure.

The plates to be welded were machined into one of the two joint configurations diagrammed in Fig. 3; a 45° single bevel or a 60° single V groove. The plates were welded with a multi-pass GTAW procedure using one of the two sets of welding conditions tabulated in Table II. Completing the single V-joint in an 0.6 in (15 mm) plate required ~35 passes at a heat input of 7 kJ/cm versus ~12 passes at a heat input of 17 kJ/cm.

Bead-on-plate welds were also made under a variety of conditions to study deposition characteristics and ferritic weld structures.

IV. Weld Characterization.

The completed welded joint was examined non-destructively by x-ray radiography using a voltage of 250 kV and a 10 mA current. No significant defects were found in these weldments.

The microstructures of the welded joints were studied by optical metallography. Polished sections were examined after etching with one of two reagents: a 5% nital solution, which reveals the solidification structure, and an acidified $FeCl_3$ solution, 200 ml HCl + 200 ml H_2O + 20 gr $FeCl_3$, which brings out the columnar grain structure and details of the transformation structure.

Bulk chemical analyses were made by Anamet Laboratories, Inc., Berkeley, California, using standard quantitative chemical techniques. High resolution chemical analyses were performed in a scanning Auger electron microscope using a voltage of 5 kV and in a scanning electron microscope equipped with energy-dispersive x-ray analysis (EDAX). This scanning electron microscope was also used for fractographic analysis of broken fracture specimens.

V. Mechanical Tests.

The mechanical tests conducted included tensile, Charpy impact and fracture toughness tests. To prepare test specimens, the welded plates were sliced perpendicular to the joint and etched with 10% nital or 2% HF solutions to reveal the weld location on the sliced surface. The specimens were then machined to have a specified location and orientation with respect to the welded joint.

The tensile tests employed subsized specimens of 0.5 in (1.27 cm) gage length and 0.125 in (0.3 cm) gage diameters, which were machined so that the gage length included base metal, HAZ material, and weld metal. Testing at 77K was done in an Instron machine equipped with a liquid nitrogen Dewar

at a crosshead speed of 0.05 cm/min. Two specimens were tested for each condition.

Charpy impact tests were performed at 300K (room temperature), 77K (liquid nitrogen temperature), and 4-5K (liquid helium temperature). The tests at 300K and 77K used ASTM standard Charpy impact specimens dimensioned and notched according to ASTM specifications (13). The impact tests at 4-5K used subsized Charpy impact specimens, 51 mm in length, which were enclosed in insulating styrofoam boxes and bathed in liquid helium until struck by the impact hammer.

The styrofoam box configuration is a slight modification of the 'lucite box' previously used in this laboratory (14). Charpy impact specimens intended to test the HAZ and fusion line toughness were notched parallel to the welding direction. Weld metal specimens were prepared both with the notch parallel to the welding direction and with the notch parallel to the weld axis as shown in Fig. 11.

Fracture toughness measurements were made on two types of specimens: pre-cracked Charpy specimens tested in three-point bending and compact tension specimens tested in tension according to ASTM specification (15). In order to minimize the deviation of the fatigue pre-crack from the desired location, the Charpy specimens were given an 8 mil saw cut of about 1 mm depth at the root of the Charpy V-notch. After fatigue pre-cracking to initial crack length to specimen width (a/w) of ~0.5, these specimens were tested in a three-point bending fixture immersed in a liquid nitrogen bath at a cross-head speed of 0.06 mm/min. The "compact tension" fracture toughness specimens were used to test the toughness of the weld metal only; they were 1.3 cm (0.51 in) in thickness and were fatigue pre-cracked to a crack length ratio (a/w) of ~0.5 in accordance with ASTM E-399 (15). These specimens

were broken at 77K under immersion in liquid nitrogen at a cross-head speed of 0.06 mm/min.

Two compact tension fracture toughness specimens of the weld metal were also tested at 4-5K, again using a stvrofoam box modification of the lucite box technique reported previously (2). Space for the compact tension specimen was hollowed out of a 25 mm thick styrofoam block and grooves were made on the inside surfaces to facilitate helium flow. The specimen assembly was wrapped and inlet holes were provided for liquid helium as described in ref. 2. The temperature during the sample cooling and testing was monitored by a Au + 0.07Fe-Chromel thermocouple embedded in the sample near the crack tip. The fracture toughness test was conducted after the sample temperature had stabilized near 4K.

None of the fracture toughness specimens tested met ASTM thickness requirements for plain strain conditions. The plain strain toughness values were hence estimated from the "equivalent energy" criterion (16). The relevant equation is

$$K_{1c} = P_q S f(a/w) \sqrt{A_1/A_2}\ [BW^3/2]^{-1} \qquad (1)$$

where a, w, B and S are respectively the crack length, specimen width, thickness and span length, P_q is the maximum load on the linear portion of the load-displacement curve, f(a/w) is the geometric shape factor (15) and A_1 and A_2 are the areas under the load-displacement curve up to the maximum load (A_1) and the load P_q(A_2). The fracture toughness values given in the following are the averages of two or more test results.

EXPERIMENTAL RESULTS

I. Weld Microstructures.

A. Bead-on-plate weldments.

A variety of test weldments were made at heat inputs ranging from 7 kJ/cm to 70 kJ/cm. These had essentially similar microstructures, which consisted of columnar grains made up of bundles of narrow solidification cells growing in the same direction. The columnar grains are revealed by chloride etching, as in Fig. 4b. They appear to grow epitaxially from half-melted coarsened grains along the fusion line. The average lateral dimension of those grains tends to increase near the center of the bead. The cellular solidification substructure of these grains is revealed by a nital etch, as in Fig. 4a. Each columnar grain contains a bundle of cells. No dendritic substructure was observed.

An examination of partially overlapped bead-on-plate weld passes showed that the solidification structure is hardly affected by the subsequent passes but the columnar grains are destroyed. The result is a fine equiaxed grain structure even at the fusion boundaries. The columnar grains or coarsened HAZ grains formed during the earlier pass did not coarsen further at the fusion boundaries of a latter pass.

B. Full-thickness weldments.

Figure 7 shows the macro- and microstructures of a completed weldment with a 7 kJ/cm heat input. The HAZ of each bead deposited reheats, recrystallizes and breaks up the original cast columnar microstructure (Fig. 5a) Thus, the whole weldment is repeatedly transformed, refined and possibly tempered during fabrication. While a few isolated islands of partially-refined structure remain (Fig. 5d), throughout the greater part of the weld volume both the coarsened HAZ and the large columnar grains are broken up

to produce a fine-grained structure. A similar grain refinement was attained with 17 kJ/cm heat input. The grain size of the irregular grains is in the range 5-10 μm in the well-refined regions.

II. Heat Simulation Results.

Figure 6 shows the microstructural changes and Fig. 7 the change in impact energy when as-annealed specimens are given rapid thermal cycles. The original as-annealed structure, Fig. 6a, has about 60μ grain size and fractures in a cleavage mode with an impact energy of ~10 ft-lb at 77K. The specimens reheated to below the A_s temperature (678°C) retained the original grain size, low toughness and brittle fracture mode. Cycling to near 800°C peak temperature destroys the original structure and creates non-uniform irregular grains (Fig. 6c). The grain size varies from 10 to 50μ. The impact toughness is dramatically improved, to ~150 ft-lb (Fig. 7), and a dimple-rupture type fracture mode is established. When the cycle reaches a peak temperature >1200°C, however, grain growth takes place (Fig. 6d) and leads to low toughness in a brittle mode (15 ft-lb). It is interesting to note the wide range of peak temperatures over which the toughness is improved, in contrast to the narrow range for conventional heat treatment, as found by Yokota, et al. (9) for the Fe-12Ni-0.5Ti alloy.

The results of the HAZ simulation done on the 2B heat-treated specimens are shown in Figs. 8 and 9. The microstructures presented in Fig. 8 document that fine grain size is retained until the peak temperature reaches about 1000°C. The Charpy impact energy is improved for peak temperatures in the range 700-1100°C, as shown in Fig. 9, and is about 50 ft-lb higher in the case of the 700°C cycle. The microstructural source of this improvement is not yet clear, but a similar behavior was found in the real HAZ Charpy impact test, as described below.

III. Mechanical Properties of the Weldments.

The measured mechanical properties of the ferritic weldments are shown in Table III along with those of the base plate (1).

A. Tensile properties.

The results of tensile tests of joints welded with filler B are shown in Table III. The tensile properties in the transverse direction compared closely with those of the base metal in the case of the 7 kJ/cm heat input but were slightly lower for the higher heat input, 17 kJ/cm. It was confirmed by etching the broken specimen that the fracture occurred outside the weld metal, perhaps near the base metal/HAZ boundary. Since the specimen was severely deformed in the fracture region, it was not possible to define an exact fracture site. The tensile data indicate that the yield strength of the weld metal is the same or higher than that of the base plate. Room temperature micro-hardness tests also give higher values in the weld metal (Hv = 290 Kg/mm^2) than in the HAZ (Hv = 280) or base metal (Hv = 260).

B. Charpy V-notch impact toughness.

Figure 10 shows the variation of impact toughness with notch location at 77K and 4.2K in the single bevel joint welded with filler B. The HAZ has the highest impact values and is about 50 ft-lb above the base plate at both 77K and 4.2K, as observed in the HAZ simulation. The weld metal also has higher impact energy than the base plate. It fractures in a ductile mode at 77K but sustains some quasi-cleavage at 4.2K.

This slight brittleness at 4.2K in the single bevel joint groove was completely suppressed in the single V joint. As shown in Fig. 11, filler B weld metal deposited in the V-joint with either of the two levels of heat input maintained high impact values at liquid helium temperature. SEM fractographs taken from broken specimens at 77K and 4.2K show a completely

ductile mode (Fig. 12). The impact DBTT of filler B weld metal was, hence, successfully suppressed to below liquid helium temperature.

As shown in Table IV, the impact toughness of filler A was much lower than that of filler B, particularly at 4.2K. The lower toughness of the filler A weld metal is, apparently, a microstructural effect. Examination of low toughness filler A specimen revealed two types of inclusion particles: a small sperical type often found inside fracture dimples in the ductile region, and a large, round or irregular type which was often observed in the brittle region. These two kinds of particles are shown in Fig. 13, with the EDAX analysis of each. The spherical particles within dimples always registered Ti and S while the irregular particles in the brittle region showed Mn, Si and Ti without any trace of S.

Table IV also shows an effect of weld geometry: the DBTT of filler A is lower than 77K in the single V joint but higher in the single bevel joint. This behavior apparently reflects the influence of weld geometry on grain refinement; the single bevel joint has a lower potential for grain refinement along the fusion boundary during multi-pass welding. Optical examination of the single bevel joint showed that the beads just beside the straight joint side retained the as-cast columnar structure, particularly near the root pass.

C. Fracture Toughness.

Since the filler A tended to become brittle at 4.2K in Charpy impact tests, further fracture toughness tests were done only on joints welded with filler B. Figure 14 shows typical load-COD curves obtained from three-point bend tests at 77K with three different locations of the fatigue crack. All the specimens seemed immune to unstable crack propagation; the specimens were fully plastic and the pre-induced cracks grew slowly in a stable manner

until the test stopped. A value of K_Q ~75 ksi $\sqrt{in}$ was computed from these curves. The fracture toughness values computed by the 'equivalent energy' method are presented in Table V.

The results of the compact tension fracture toughness tests of weld metal at 77K and 4-6K are also shown in Table V and Fig. 15. The crack in the compact tension specimen grew in a stable manner at 77K but at 4-6K gave a serrated load-deflection curve up to the maximum load, then propagated discontinuously (Fig. 15). This behavior was also observed in the base metal, as reported previously (2). The calculated K_q values were 138 ksi $\sqrt{in}$ at 77K and 115 ksi $\sqrt{in}$ at 4-6K. Whatever the testing method at 77K, the estimated fracture toughness of the weld metal is comparable with the toughness of the base plate (307 ksi $\sqrt{in}$) and that of the HAZ is slightly higher. A lower boundary for the fracture toughness of the 4-6K specimens was calculated using equation 1. The area under curve, A_1, was taken to the maximum load point. The calculated K_{1C} value was ~160 ksi $\sqrt{in}$, average of two tests. Examination of the fracture surface along the fatigue crack line revealed that the fracture mode was a mixture of dimple rupture and quasi-cleavage as shown in Fig. 16.

DISCUSSION

The results presented above establish that grain-refined 12Ni steel can be welded with ferritic filler metal so that both high yield strength and excellent toughness are retained in the base plate, heat-affected zone, and weld metal at temperatures as low as 4K. This success may make it possible to realize several advantages of ferritic weldments in cryogenic structures, including high strength, a complete joint at the fusion boundary, matching low thermal expansion, and the low cost of ferritic consumables. The success of the welding procedure seems attributable to a combination of microstructural

refinement through the multi-pass welding process and the low interstitial weld deposit of the GTAW.

The weldments used differ from the base plate in composition and thermal history:

I. Weld metal chemistry.

The weld metal chemistry explored in this work differs from that of the base plate in three respects: the increased Ni content, the addition of Mn and Si (filler A) and the addition of boron (filler B).

(a) Nickel content. The nickel content was increased to 14 wt.% to err on the side of safety in achieving a low DBTT in the weld metal. It is not clear that this increase is necessary. While a satisfactory DBTT was obtained, the thermal cycle simulation studies suggest that satisfactory properties might also have resulted had the base metal composition been used.

Current metallurgical understanding does not permit an a priori choice of an optimum nickel content for low temperature toughness. While an increase in nickel content is often found to lead to a decrease in the DBTT (9,10), the mechanism of the effect is uncertain, and it is likely that the primary benefit achieved from nickel is indirect, through the influence of nickel on the response of the microstructure to thermal treatment. Previous research suggests, however, that there is an optimum nickel content of the weld filler metal which lies somewhat above that of the base plate. In the GTA welding of 9Ni steel an increase in nickel content from 5 to 11 wt.% gave a monotonic improvement in toughness at 77K (17), but toughness deteriorated when the nickel content was increased further to 17 wt.%. The problem at higher nickel content may be associated with an unstable austenite retention in the weldment, as is apparently the case in 18%Ni (250 grade) maraging steel (18).

B. Manganese and silicon.

Manganese and silicon are common deoxidizers which were added to filler metal "A" in this research to determine their effect on the final weldment properties. Their presence led to a deterioration in the weld metal toughness, which seems to be clearly associated with the formation of large (Mn-Si) oxides. These results are in general agreement with previous research. Silicon is often intentionally added to ferritic weldments for 9Ni steel (19) since 9Ni contains a significant alloying addition of manganese, and it is known that a low Mn/Si ratio is needed to obtain efficient removal of deoxidation products to the weld surface (20). Moreover, serious porosity problems have been encountered in ferritic GMA welding of 9%Ni steel with Si-free weld metal (21) and in the welding of low carbon manganese steels (20), apparently because of insufficient deoxidation in the weld deposit. It has, however, been found that both Si and Mn decrease the low temperature toughness of welded 9Ni steel (17). With Si-containing weld chemistries, large (Mn,Si) oxides have been found on the fracture surfaces of ferritic weldments in 9Ni steel (22), and apparently cause embrittlement by mechanisms similar to that noted in the present work.

The results obtained with filler metal "B" in the present work show that manganese and silicon are not necessary alloy additions to the weld metal. The 12Ni base plate alloy contains no manganese, and deoxidation and scavenging is, apparently, efficiently accomplished by the alloy addition of Ti, as was inferred by previous researchers (1,10). As shown in the Auger analysis of inclusion particles presented as Fig. 17, Ti acts as a deoxidizer and combines with carbon and sulfur to getter other potentially deliterious elements. Given the relative cleanliness of the GTA welding process, the titanium content of the base alloy seems sufficient to ensure a clean and well gettered weldment.

C. Boron.

Boron was added to filler metal "B" in the expectation that it would act as a strong surfactant in boundaries of the weld metal to improve grain refinement and prevent intergranular separation, as it does in other alloys (11,12). Its actual role in the weldment has not been identified since no trace of boron was detected by Auger analysis of the microstructure or fracture surface. Boron did, however, seem to be beneficial to the welding process. The addition of a small amount of boron to the Fe-12Ni-0.25Ti base plate improved weld metal fluidity in bead-on-plate welding, and it was found that filler "B", which contained 30 ppm boron, produced a more easily controlled weld puddle and better weld beads than did the boron-free filler "A".

II. Effect of Weld Thermal Cycles.

The high impact toughness and the low ductile-brittle transition temperature of the weldment is a consequence of the multi-pass GTA welding process, which appears to refine the grain size of the weld deposit and to retain fine grain size in the heat-affected zone. A detailed transmission electron microscopic analysis of the consequences of the multi-pass GTA process is now in progress. Some important aspects of the grain refinement are, however, clear from the evidence obtained in the work reported here.

In the conventional treatment of ferritic $\frac{\text{Fe-Ni}}{\text{cryogenic}}$ steels there are two mechanistically different ways of establishing a fine effective grain size: the direct crystallographic refinement of the martensite or ferrite structure, and the introduction of a fine distribution of precipitated austenite which serves to break up the crystallographic alignment of the martensite or ferrite structure. In the present case it appears that the grain refinement mechanism is direct crystallographic refinement of the deposit, since no measurable retained austenite is detected in the weldment or

heat-affected zone, even at room temperature. This result is in agreement with previous Lawrence Berkeley Laboratory research on the GMA welding of 9%Ni steel with ferritic filler metals (21), but is at variance with the results of similar research by Tamura, et al. (23), who reported a significant amount of thermally stable austenite (approximately 6%) in the weld metal, and suggested a correspondence between this austenite and the improvement in impact toughness. The improvement in toughness obtained in the present work is associated with microstructural changes in the ferritic deposit during the fast heating and cooling cycles associated with multi-pass welding.

There is a reasonable body of prior research showing that a rapid austenitizing cycle can accomplish a significant grain refinement of steel and improve its mechanical properties with respect to conventionally treated material. This research involved iron-carbon alloys (24,25) and HY-130 steel (5Ni-Cr-Mo-B) (26). The research by Porter, et al. (26) on HY-130 steel is particularly relevant, since these workers found that the degree of grain refinement increased with heating rate and also noted changes in dislocation substructure which were more pronounced in specimens given a rapid thermal cycle. The reheating rate in multi-pass GTA welding is quite rapid and was shown above to lead to an apparent grain size in the 5-10 μm range. The substructural changes caused by the rapid thermal cycle must, however, also be important since the 5-10 μm apparent grain size of the weldment is considerably above that (less than 1 μm) which appears to be necessary to lower the ductile-brittle transition of the base plate below 4.2K in conventional heat treatments.

III. Alternative Welding Processes.

The GTAW welding process was selected for the present research because of its cleanliness and its controllability. In addition, the large, uniform

heat-affected zone of the GTA process is useful to insure the cyclic heat treatment of previously deposited material.

This advantageous combination is not easily achieved in other welding processes such as gas metal arc (GMA) or electron beam (EB) welding. A conventional electron beam welding has already been demonstrated (4) to be inappropriate because of the coarse solidification structure established in the weld metal. The GMA process is also difficult to effect, but deserves further exploration because of the economic benefits to be achieved from its higher deposition rate.

The gas metal arc welding process suffers from two shortcomings: the localization of its heat-affected zone due to its high deposition rate and its bell-like bead shape, and its relatively high contamination, particularly by oxygen and nitrogen, which arises from plasma jet instabilities in the consumable electrode process. Zanis, et al. (27) considered the problem of achieving grain refinement in a high-rate deposition GMAW process and have proposed reheatment treatments using heating sources such as autogeneous GTAW or lasers to refine the GMA deposit. Dolby (28) has also proposed in-process techniques to refine the microstructure of weld deposits. But the contamination problem must also be overcome. Watanabe, et al. (29) investigated the notch toughness of ferritic SMAW weld metal and found that the toughness decreased dramatically when the oxygen content rose above 100 ppm. Further research will be necessary before the GMAW can be successfully used for welding ferritic steels with ferritic consumables for deep cryogenic applications.

CONCLUSION

A. The GTAW process can be successfully used to weld grain-refined Fe-12Ni-0.25Ti alloys with ferritic filler metal so that matching strength

is obtained in the weldment and excellent toughness is retained even at 4K in both the weld metal and the heat-affected zone.

B. The promising properties obtained depend on two factors: the chemical cleanliness of the weldment achieved in the GTAW process, and the microstructural refinement of the weldment and retention of microstructural refinement in the heat-affected zone, due to rapid thermal cycling of the weld region by the multi-pass GTAW process.

ACKNOWLEDGEMENT

This work was supported by the Director, Office of Energy Research, Office of Development and Technology, Magnetic Systems Division of the U. S. Department of Energy under Contract Number W-7405-ENG-48.

REFERENCES

1. Jin, S.; Morris, Jr. J.W.; and Zackay, V.F.: Grain refinement through thermal cycling in an Fe-Ni-Ti cryogenic alloy. Metallurgical Trans. 6A (1) 1975, pp. 141-149.
2. Jin, S.; Hwang, S.K.; and Morris, Jr. J.W.: Comparative fracture toughness of an ultrafine grained Fe-Ni alloy at liquid helium temperature. Metallurgical Trans. 6A (8) 1976, pp. 1569-1575.
3. Syn, S.K.; Jin, S.; and Morris, Jr. J.W.: Cryogenic fracture toughness of 9Ni steel enhanced through grain refinement. Metallurgical Trans. 7A (12) 1976, pp. 1827-1832.
4. Williams, D.E.: The weldability of thermally grain-refined Fe-12Ni-0.25Ti for cryogenic structural applications. M.S. thesis, University of California Berkeley, Berkeley, CA. 94720, 1979.
5. Ishikawa, K.; and Maruyama, N.: Fracture and strength of mig welded Fe-13%Ni-3%Mo alloy for cryogenic service. Cryogenics, 18 (10) 1978, pp. 585-589.
6. Watanabe, M.; and Watanabe, I.: Brittleness at bonded part of deposited metal by austenitic stainless steel electrode to the ferritic mother metal. IIW Doc. No. X-511-69, 1969.
7. Nippon Kokan K.K.; and Kobe Steel, LTD.: Matching ferritic consumable welding of 9% nickel steel to enhance safety and economy. Practicability of ferritic filler for welding 9%Ni steel plates. 1980 AWS 61st Annual Meeting, Session 22, 1980.
8. Devletion, J.H.; Stephens, J.R.; and Witzke, W.R.: Weldability of high toughness Fe-12%Ni alloys containing Ti, Al or Nb. Welding Journal 56 (4) 1977, pp. 97-2 to 102-s.
9. Yokota, M.J.; Sasaki, G.; and Horwood, W.A.: Developing high impact toughness

(Yokota Cont.)

in Fe-Ni alloys at liquid nitrogen temperature. Materials Science and Eng. 19 (1) 1975, pp. 129-138.

10. Ishikawa, K.; Maruyama, N.; and Tsuya, K.: Fracture toughness of Fe-13%Ni-3%Mo-0.2%Ti alloy at cryogenic temperature. Tetsu-to-Hagane, 64 (7) 1978, pp. 1038-1046.

11. Hwang, S.K.; and Morris, Jr. J.W.: The use of a boron addition to prevent intergranular embrittlement in Fe-12Mn. Metallurgical Trans. 11A (7) 1980 pp. 1197-1206.

12. Devletian, J.H.; and Heine, R.W.: Grain refining effect of boron in carbon steel welds. Welding Journal 52 (12) 1973, pp. 529-s to 536-s.

13. ASTM Standard Designation E-23.

14. Jin, S.; Horwood, W.A.; Morris, Jr. J.W.; and Zackay, V.F.: A simple method for Charpy impact testing below 6K. Advances in Cryogenic Eng. 19, 1974 pp. 373-378.

15. ASTM Standard Designation E399-75, 1975.

16. Witt, F.J.; and Mager, T.R.: Procedure for determining bounding values on fracture toughness K_{1c} at any temperature. ORNL-TM-3894, Oak Ridge National Laboratory.

17. Kobe Steel, LTD: Practical application of welding procedures of ferritic filler to 9%Ni steel plates for cryogenic storage tanks. No. RDPD-7902, October, 1979.

18. Paley, Z.: The heat treatment of 18Ni Maraging steel weld metal. Welding Journal 48 (6) 1969, pp.245-2 to 252-s.

19. Mahin, K.W.; Morris, Jr. J.W.; and Watanabe, I.: A review of the development of ferritic consumables for the welding of 9%Ni steel: Research in the United States and Japan. Advances in Cryogenic Eng. 26, 1980, pp. 187-199.

20. Widgery, D.J.: Deoxidation practice for mild steel weld metal. Welding Journal 55 (3) 1976, pp. 57-s to 68-s.

21. Mahin, K.W.; and Morris, Jr. J.W.: A study of ferritic weld deposits in Fe-9Ni steel. Advances in Cryogenic Eng. 26, 1980, pp. 210-218.

22. Mahin, K.W.: Characterization of ferritic GMA weld deposits in 9%Ni steel for cryogenic applications. Ph.D. thesis, University of California, Berkeley, Berkeley, CA. 94720, 1980.

23. Tamura, H.; Onzawa, T.; Uematsu, S.; and Meakawa, S.: Notch toughness and retained austenite in 9%Ni steel welds matched ferritic filler metals: Report I. Studies on retained austenite in cryogenic steel welds. Journal of Japan Welding Society 48 (11) 1979, pp. 931-936.

24. Grange, R.A.: The rapid heat treatment of steel. Metallurgical Trans. 2 (1) 1971, pp. 65-78.

25. Mahajan, S.W.; Venkataraman, G.; and Mallik, A.K.: Grain refinement by cycling rapid heating. Metallography 6 (4) 1973, pp. 337-345.

26. Porter, L.F.; and Dabkowski, D.S.: Ultrafine Grain Metals, eds. Burke, J.J. and Weiss, V., Syracuse University Press, Syracuse, N.Y. 1969.

27. Zanis, C.A.; Holsberg, P.W.; and Dunn, Jr. E.C.: Seawater subcritical cracking of HY-steel weldments. Welding Journal 59 (12) 1980, pp. 355-s to 363-s.

28. Dolby, R.E.: HAZ toughness of structure and pressure vessel steels--Improvement and prediction. Welding Journal 58 (8) 1979, pp. 225-s to 238-s.

29. Watanabe, M.; Tanaka, J.; and Watanabe, I.: Ferritic filler material for gas-shielded metal-arc welding of 9% nickel steel. Welding and Metal Fabrication 41 (5) 1973, pp. 167-176.

Table I. Compositions of base metal, filler metals and weld deposits.

Element		Fe	Ni	Ti	Mn	Si	P	S	O	N	B	C
Base Metal		bal.	12.07	0.20	—	—	0.001	0.002	<0.001	<0.001	—	0.002
Filler Metal	A	bal.	14.04	0.21	0.37	0.09	0.005	0.002	0.005	<0.001	—	0.006
	B	bal.	13.87	0.16	—	—	0.001	0.002	0.006	<0.001	0.003	0.003
Weld Deposit	A	bal.	13.98	0.20	0.33	0.08	0.005	*	0.007	0.007	—	0.003
	B	bal.	13.81	0.15	—	—	*	*	0.007	0.006	0.0027	0.003

* Not Analyzed

— Negligible

XBL 808-5755

TABLE II. Welding Conditions.

Heat Input (kJ/cm)	7-8	17-18
Arc Voltage (V)	14-18	18-20
Welding Current (A)	150-180	250-300
Welding Speed (cm/sec)	0.4	0.4
Shielding Gas Flow Rate	Pure argon, 25 ft^3/hr	
Root Gap	Same as rod diameter	
Interpass Temperature	50-150°C	

TABLE III. Results of tensile tests at 77K.

Specimen	Heat Input kJ/cm	Y.S. ksi	T.S. ksi	Elongation (%)	R.A. (%)
Fe-12Ni-0.25Ti (Base Metal)		149	154	26.8	72.1
Welded Joint* (Base/HAZ/WM)	7	145	154	25.0	71.0
	17	140	148	21.2	68.0

* All specimens were fractured near Base/HAZ boundary.

TABLE IV. Charpy impact toughness (ft-lb) with different joint configurations.

Weld Metal	Testing Temp. (K)	Single Bevel	Single V
Filler A	77.0	70	123
	4.2	27	53
Filler B	77.0	122	135
	4.2	97	128

TABLE V. Fracture toughness at cryogenic temperatures.

All values were obtained by "Equivalent Energy" method.

Testing Temp.	Heat Input	Three-point Bend ($ksi\sqrt{in}$)		Compact Tension ($ksi\sqrt{in}$)
		Weld Metal	HAZ	Weld Metal
77K	7	324	-	-
	17	286	330	280
4.2K	17	-	-	160

FIGURE CAPTIONS

1. 2B heat treatment with Fe-Ni equilibrium phase diagram.
2. Thermal cycle curve for the simulation of 1300°C peak temperature.
3. Joint configurations.
4. Microstructures of bead-on-plate welds etched with (a) 5% Nital, (b) acidified $FeCl_3$ solution.
5. Macro- and microstructures of full thickness welded joint with heat input 7 kJ/cm.
6. Microstructural changes of annealed specimen with various peak temperatures.
7. Variation of Charpy impact energy at 77K with peak temperature of simulated weld cycle.
8. Microstructural changes of 2B base metal with various peak temperatures.
9. Charpy impact energy variation of simulated HAZ at 77K.
10. Variation of impact toughness with notch location at 77 and 4.2K.
11. Variation of Charpy impact energy of filler B with testing temperature, heat input and notch orientation.
12. SEM fractographs: Charpy specimens broken at 77 and (b) 4.2K.
13. SEM fractographs of filler A weld metal in (a) ductile and (b) brittle region with EDAX analysis of each particle.
14. Load-COD curves for fracture toughness tests at 77K.
15. Load-COD curves of weld metal in compact tension tests at 77 and 4.2K.
16. SEM fractograph of compact tension specimen tested at 4.2K.
17. Scanning Auger microprobe spectra of the particles inside the fracture dimples in filler A weld metal.

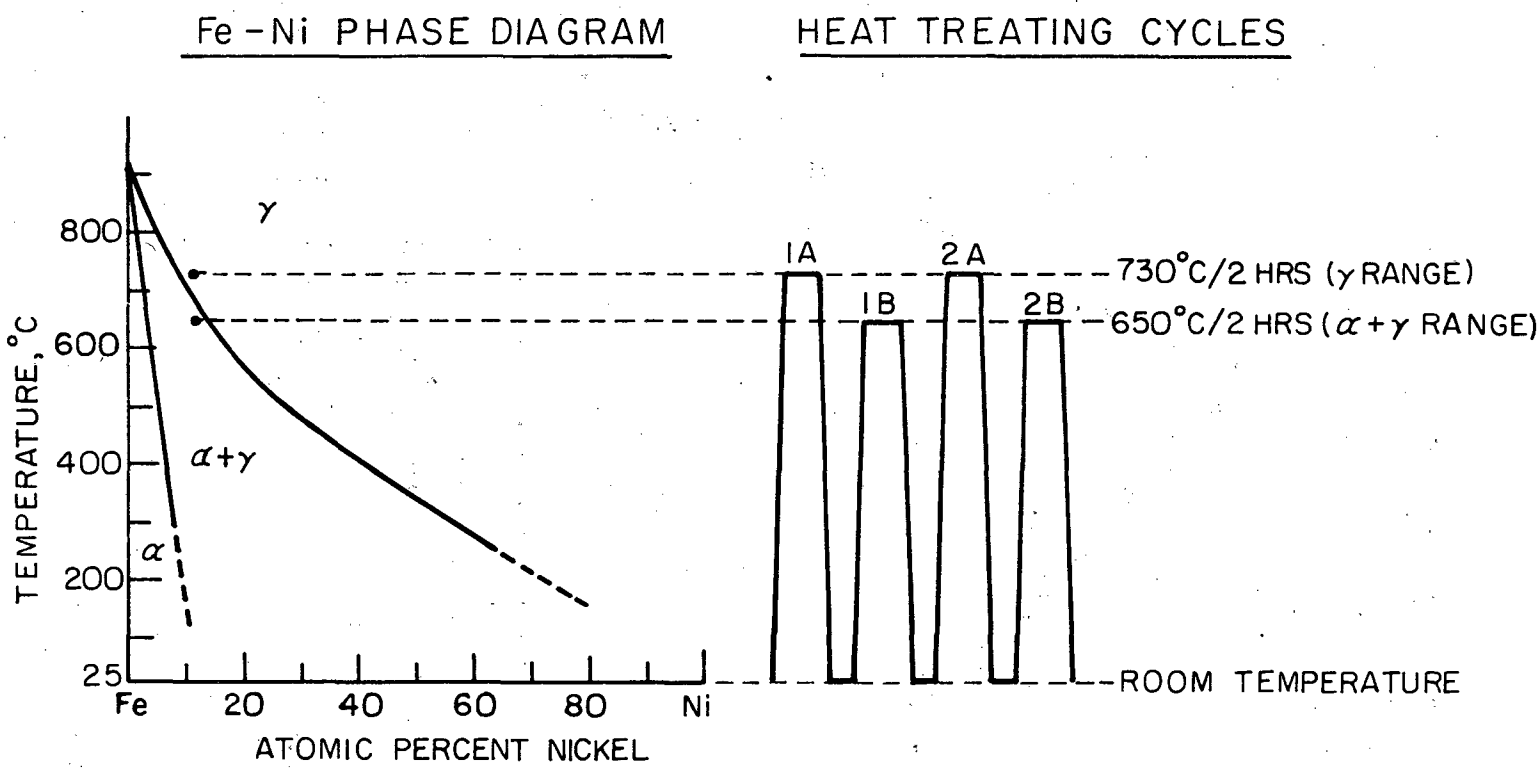

Figure 1

XBL 739-1884

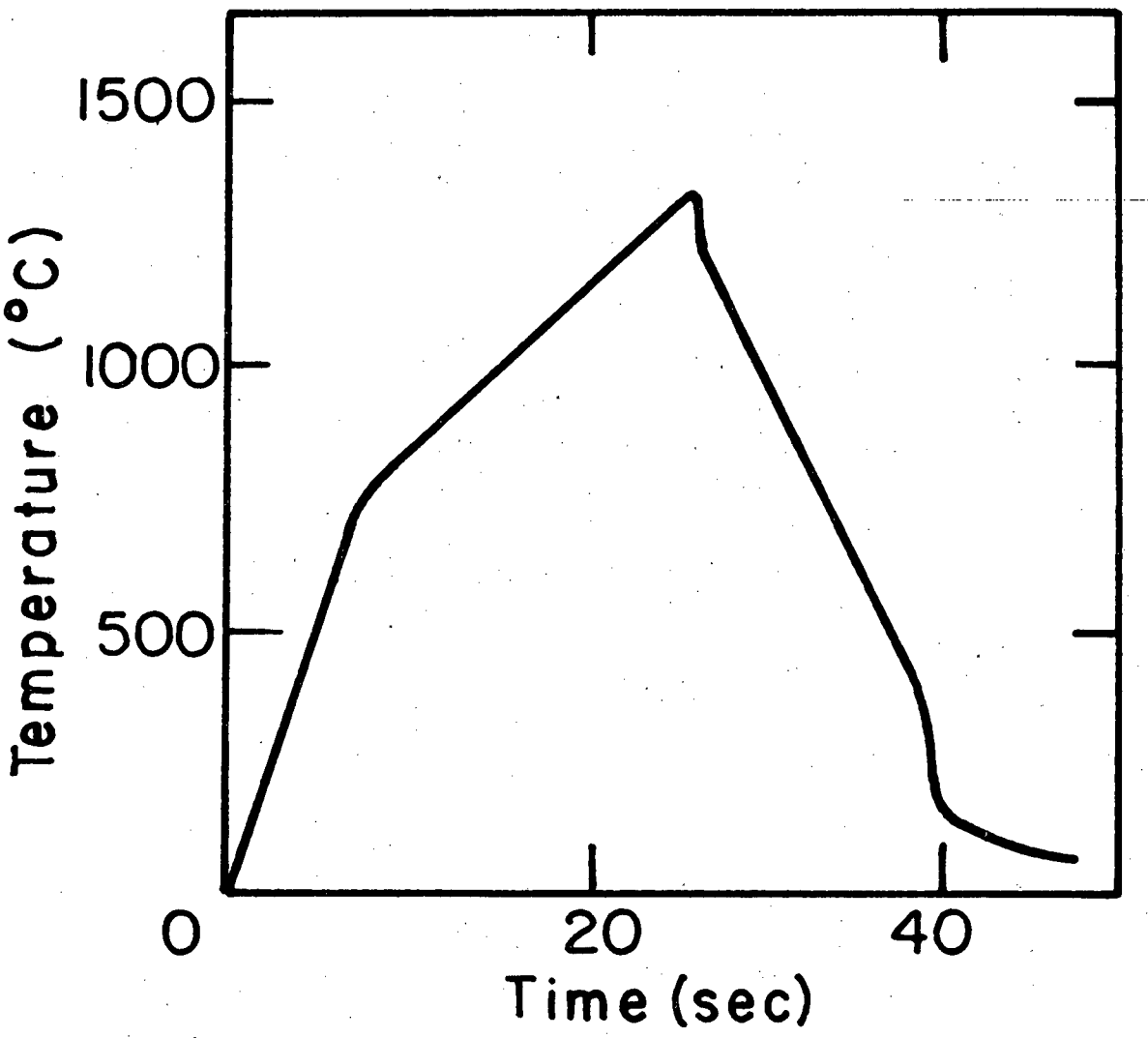

Figure 2

XBL 803-4799

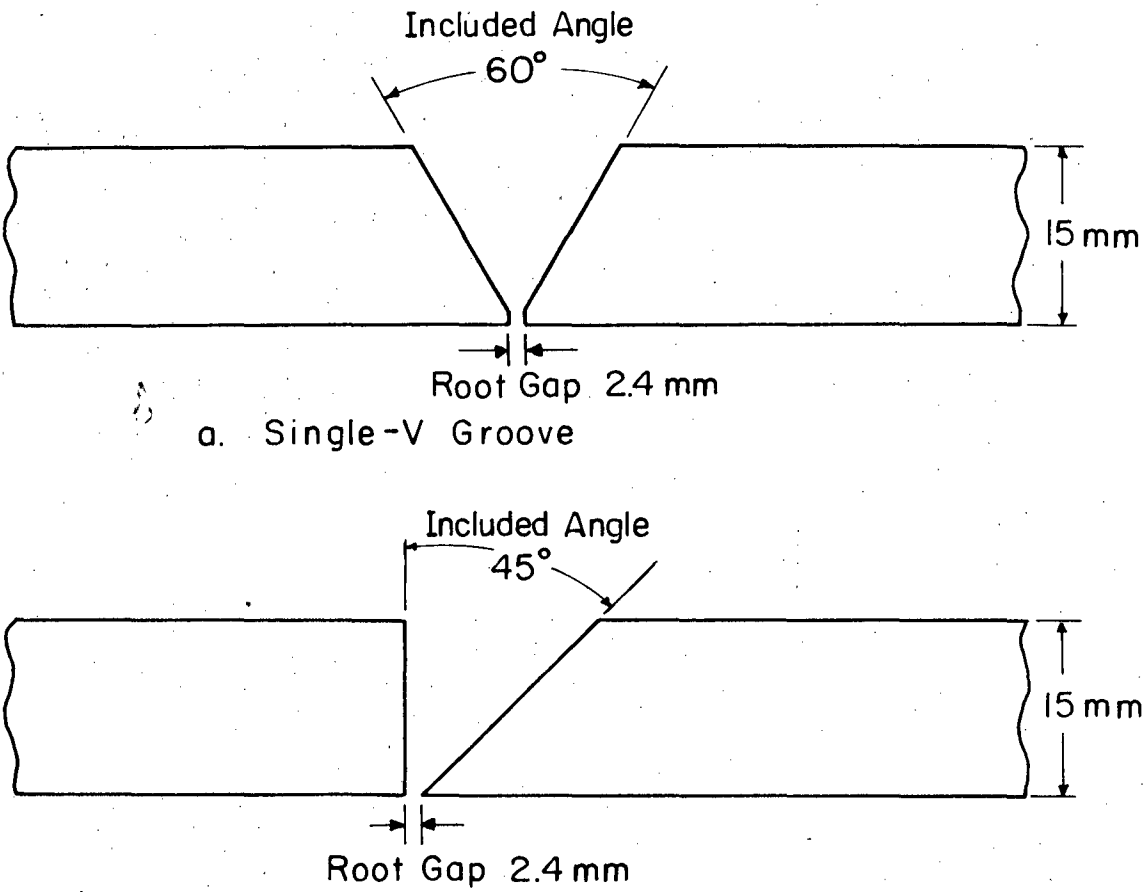

Figure 3

XBL 808-5754

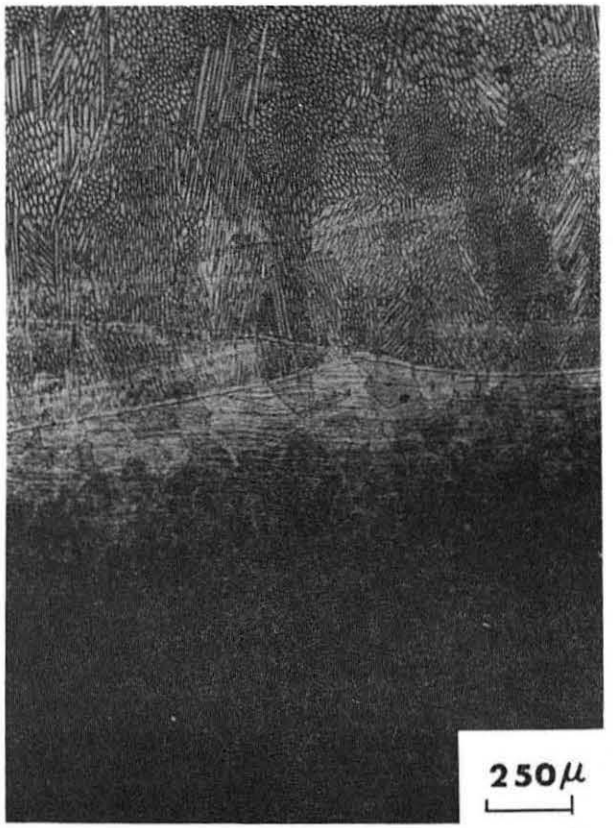

5% Nital

Acid. $FeCl_3$

Figure 4

XBB 802-1882

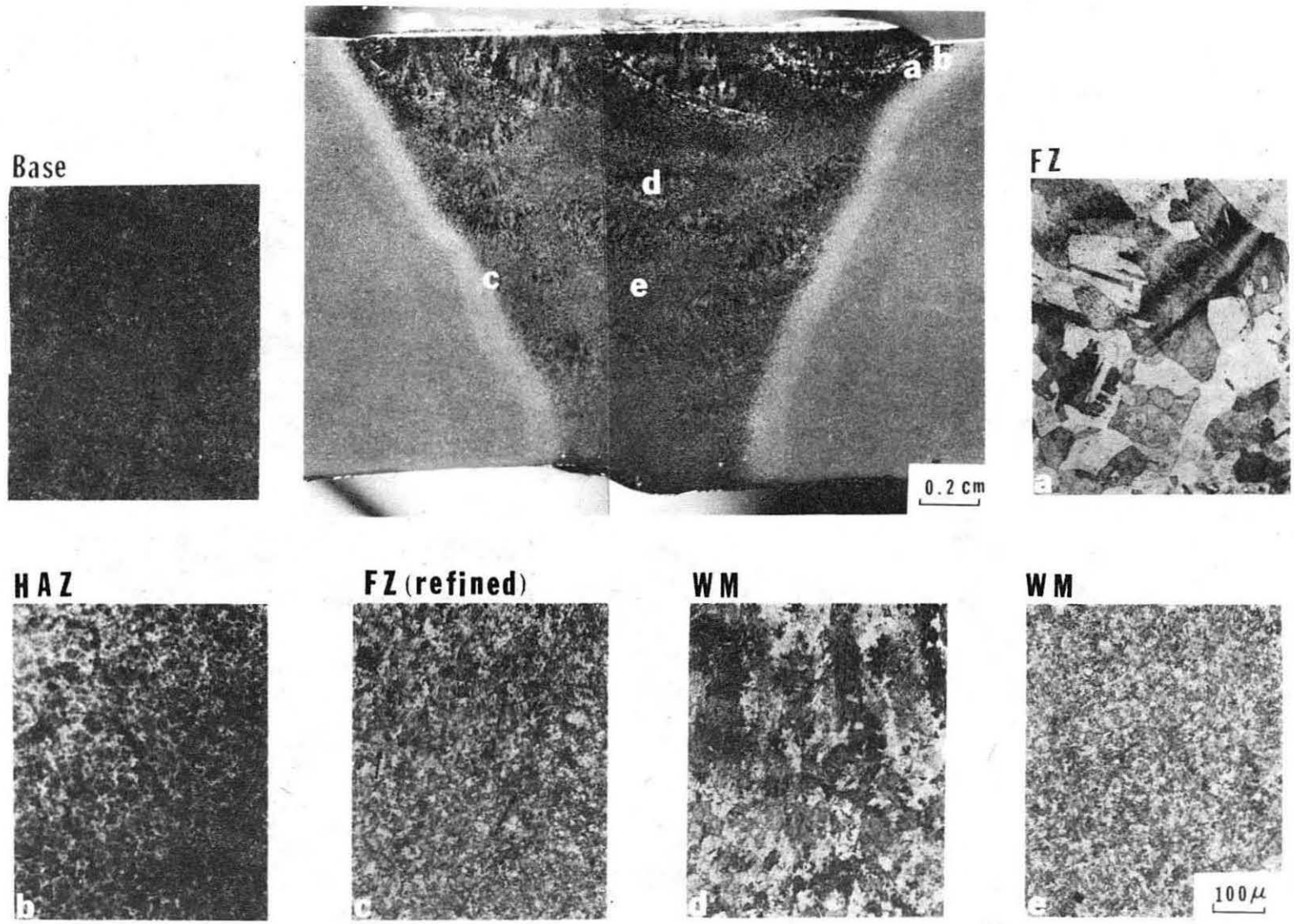

Figure 5

XBB 805-5473A

PEAK TEMPERATURE vs. GRAIN SIZE

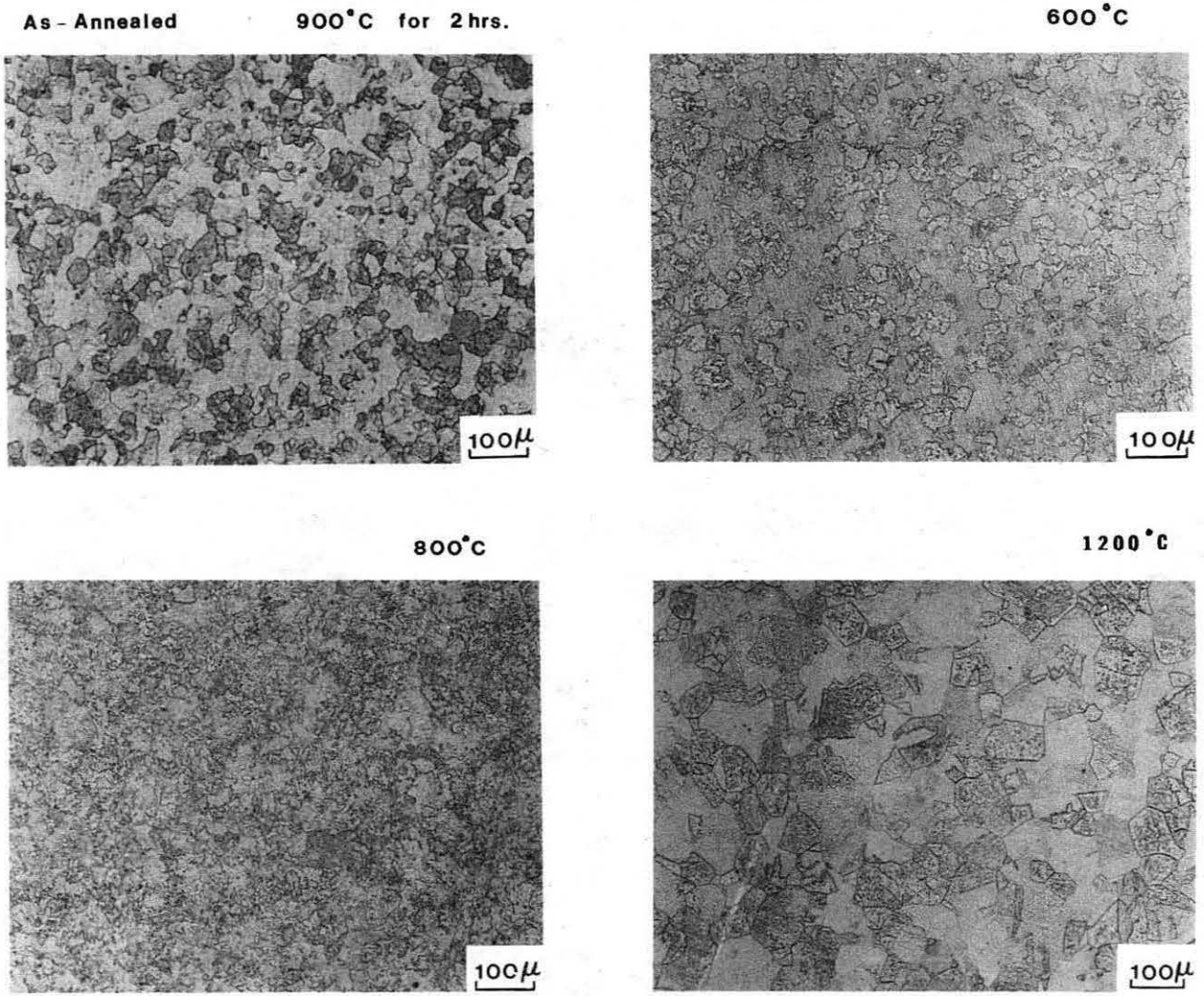

Figure 6

XBB 799-12638

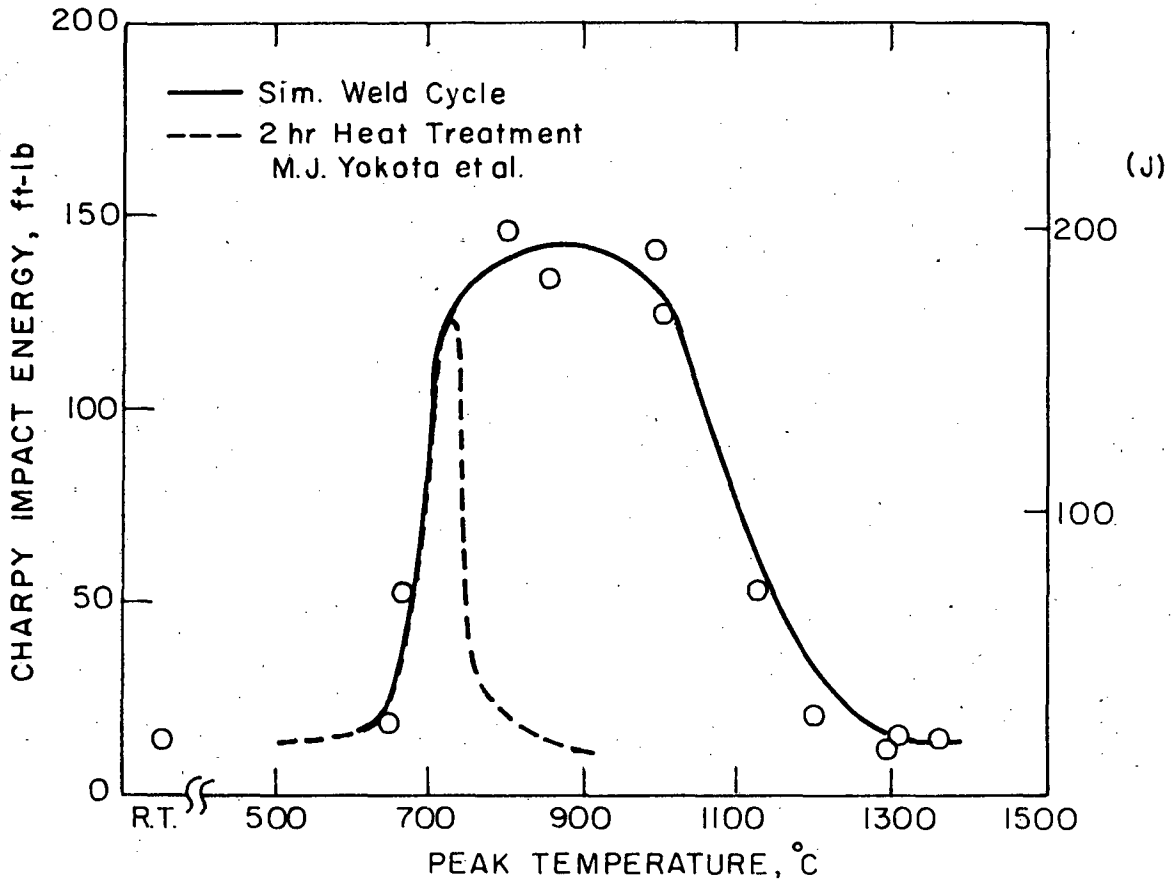

Figure 7

XBL809-5979

Heat Simulation of HAZ

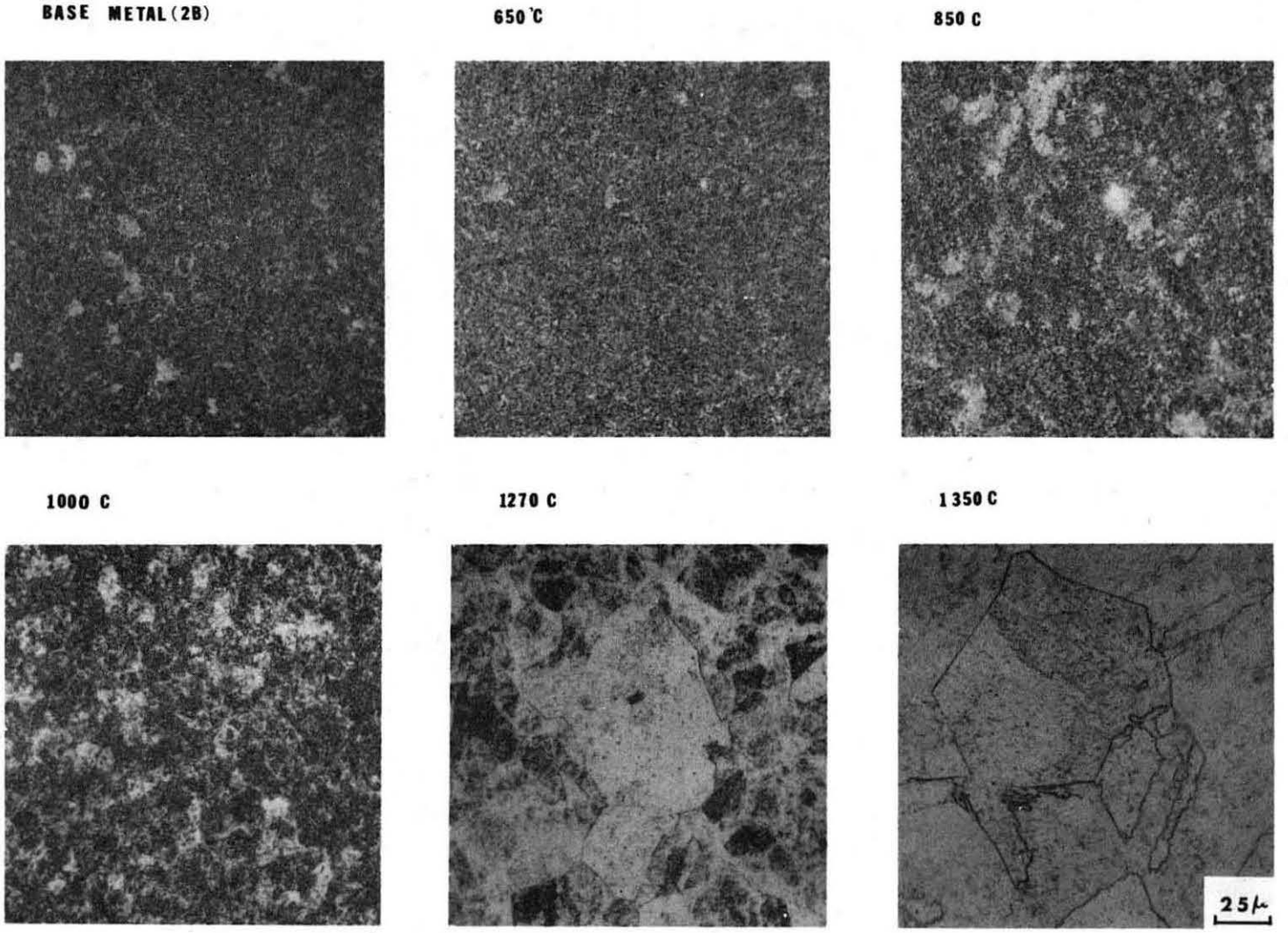

Figure 8

XBB 805-5474

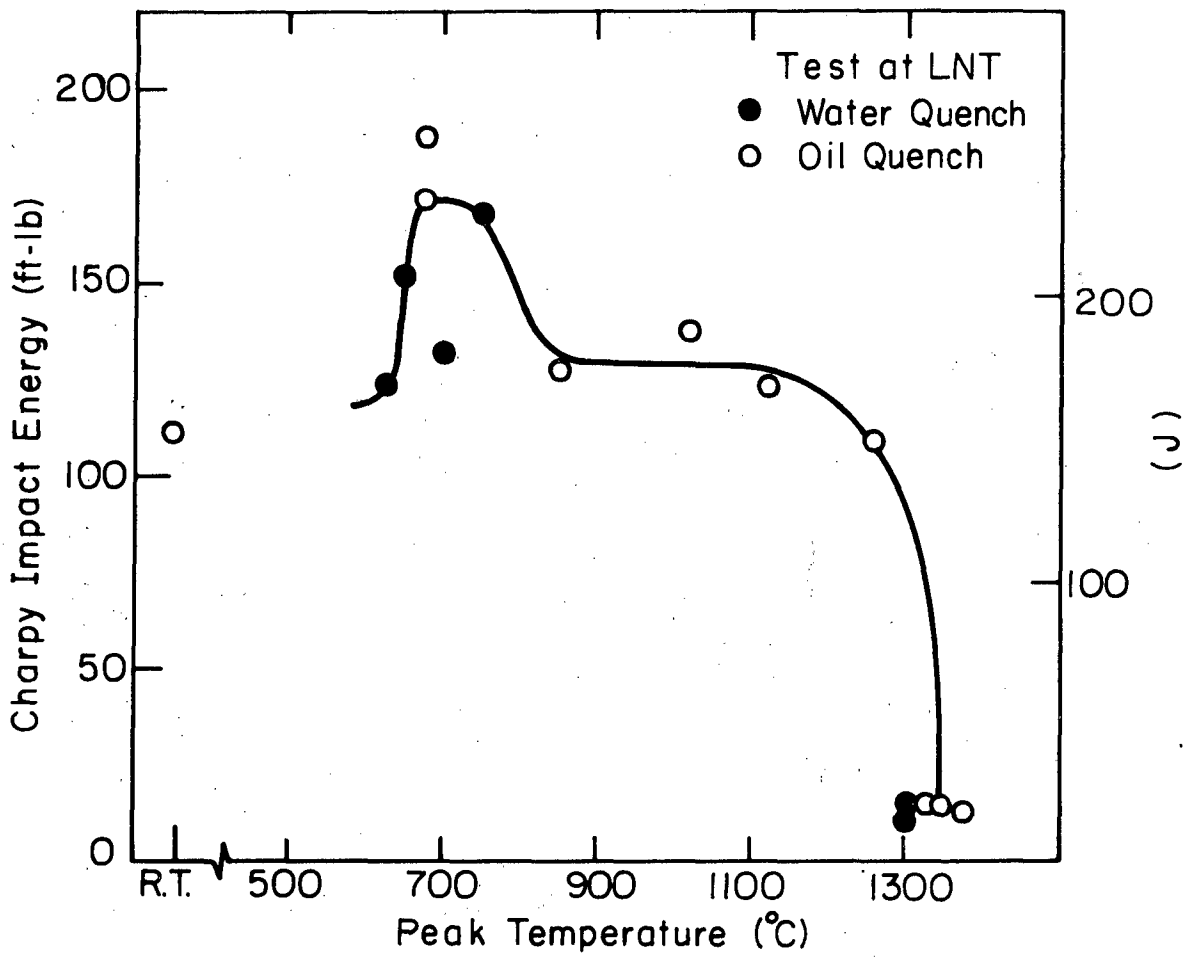

Figure 9

XBL 805-5189

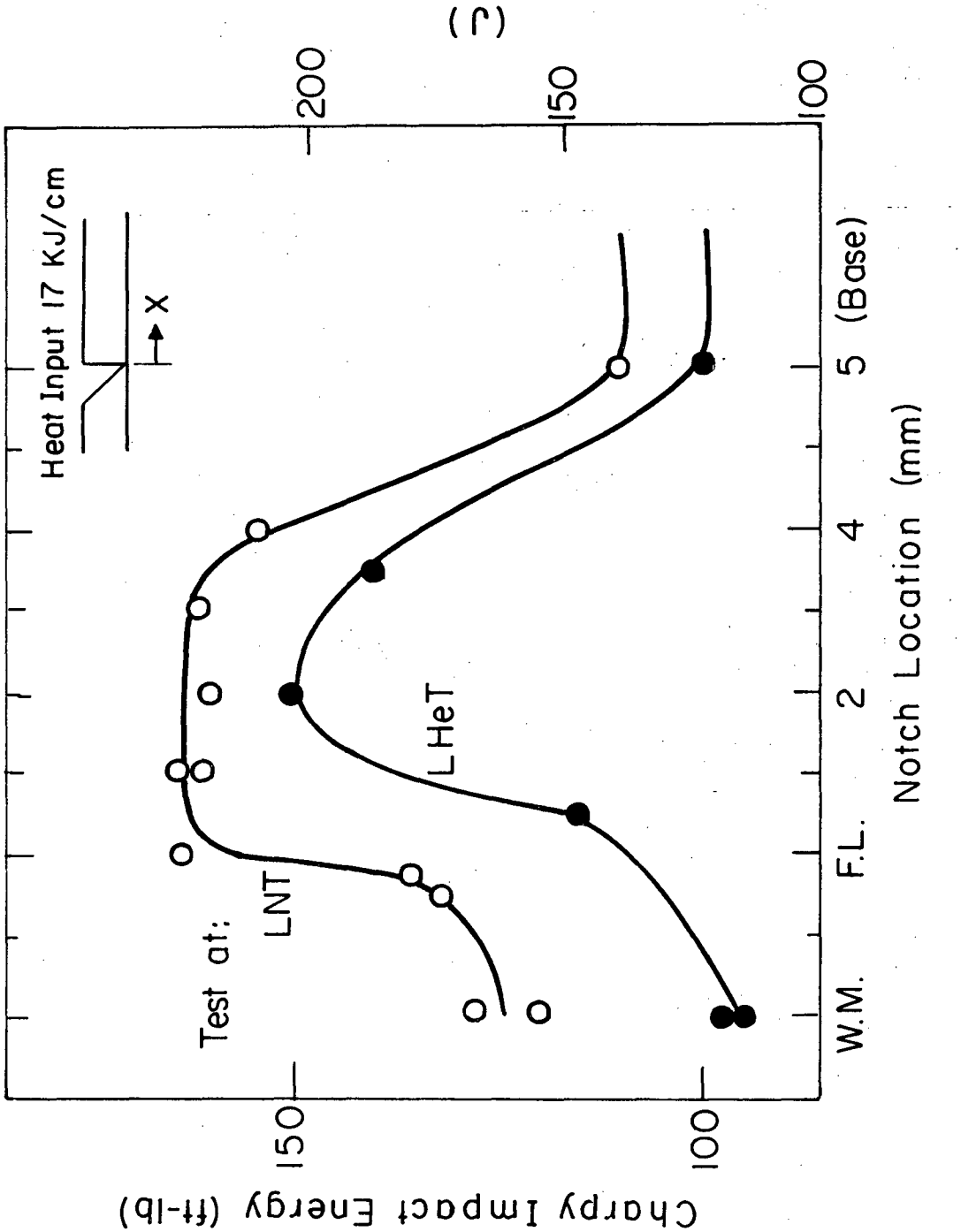
Charpy Impact Energy (ft-lb)
150
100
200
150
100
W.M.
F.L.
2
4
5 (Base)
Notch Location (mm)
Test at:
LNT
LHeT
Heat Input 17 KJ/cm
X
(c)
XBL813-5392

Figure 10

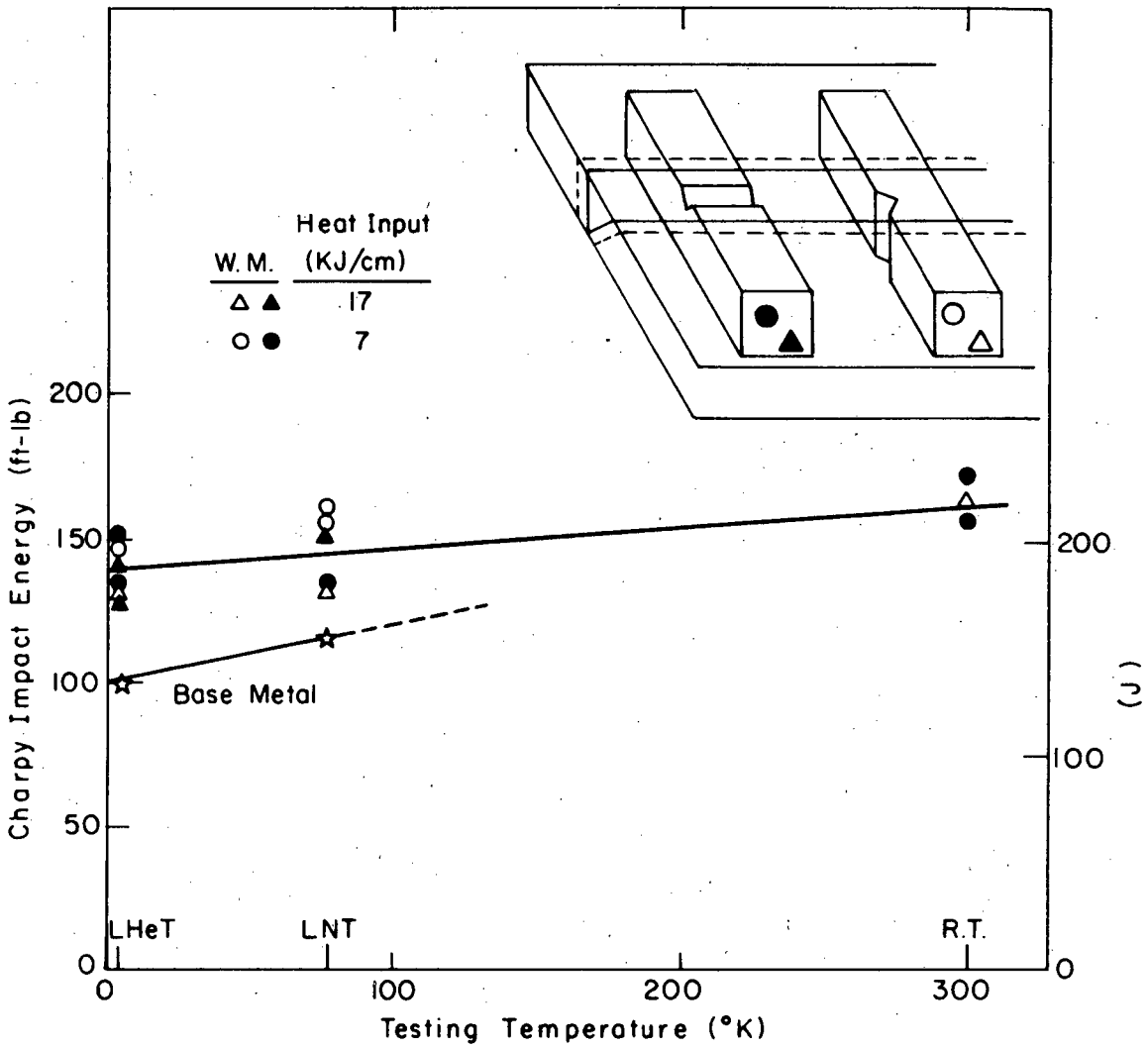

Figure 11

XBL 814-5458

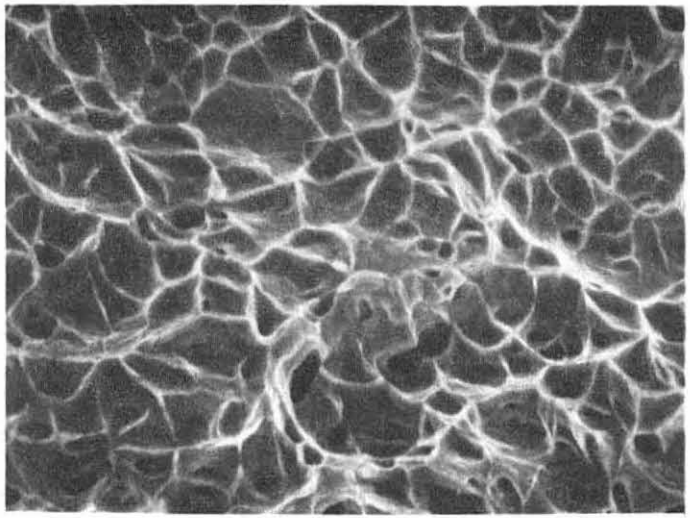

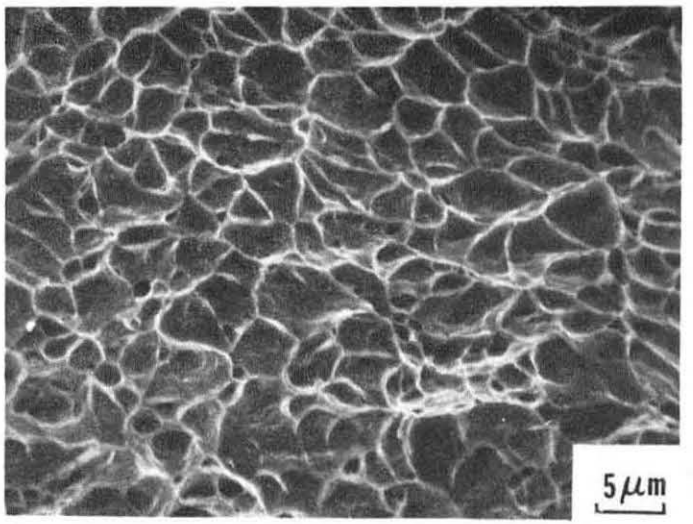

XBB 809-10455

LNT C_V

LHeT C_V

Figure 12

Heat Input 17 (Kj/cm)

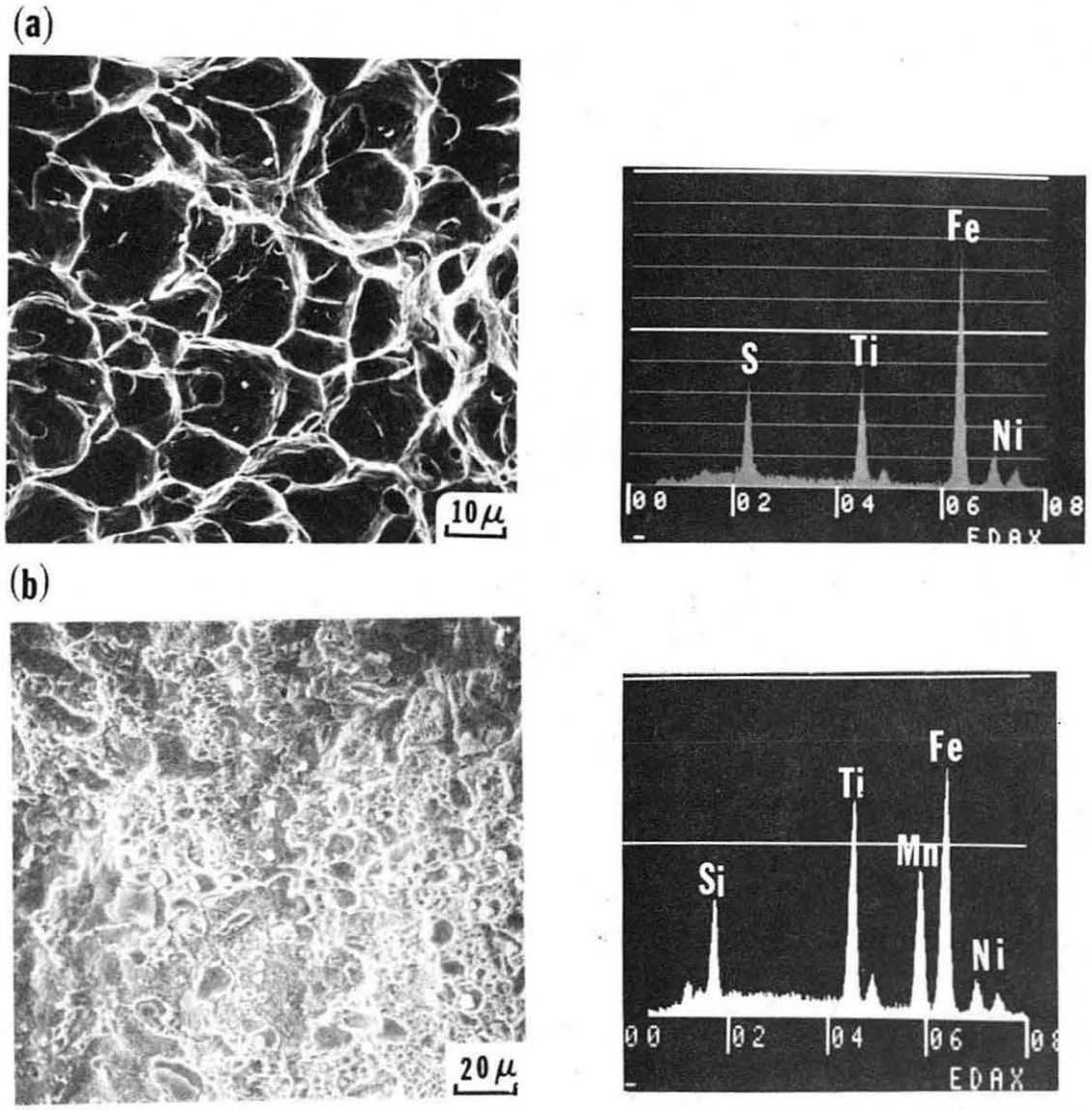

XBB 817-6675

Figure 13

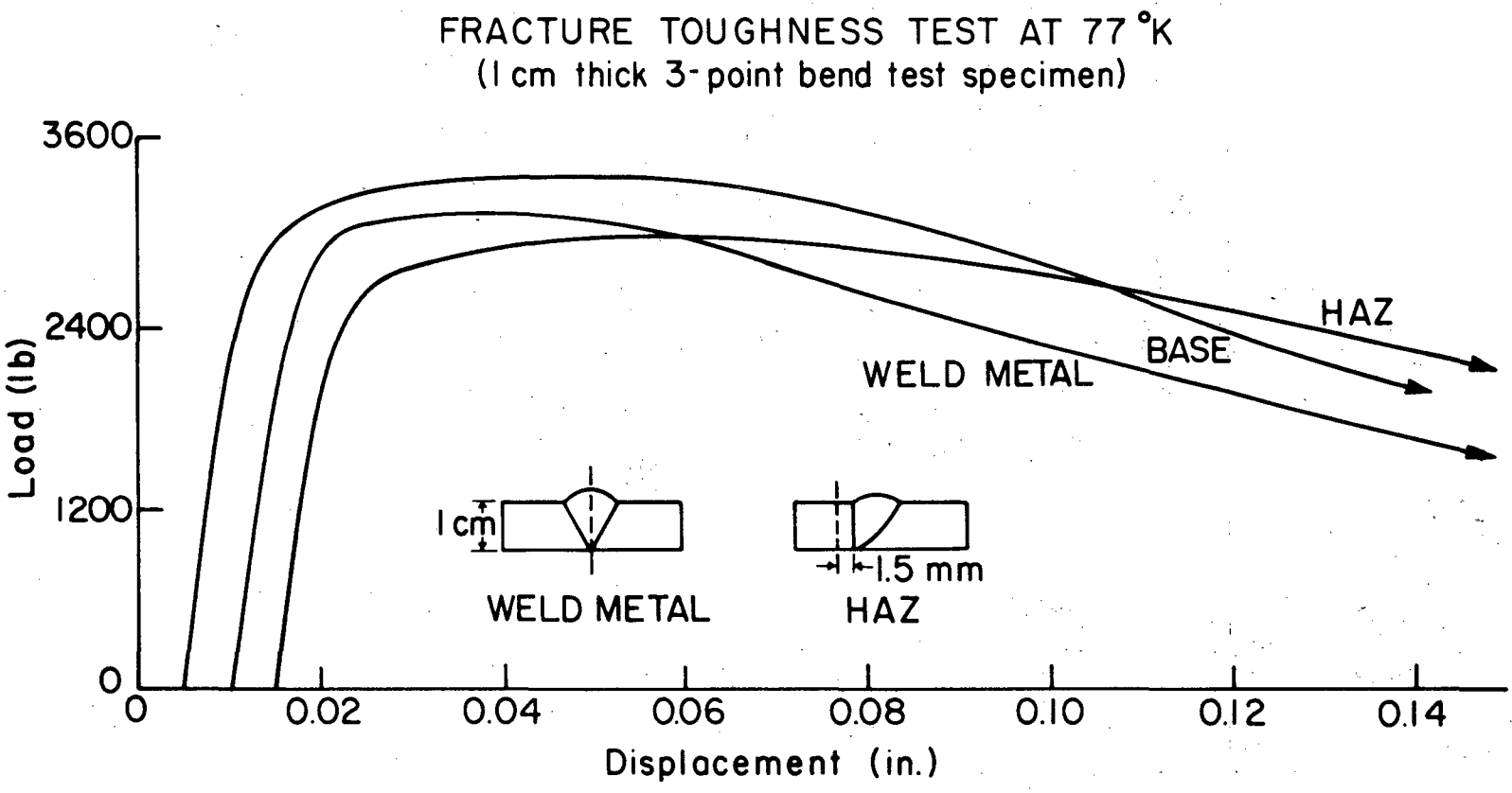

Figure 14

XBL 815-5690

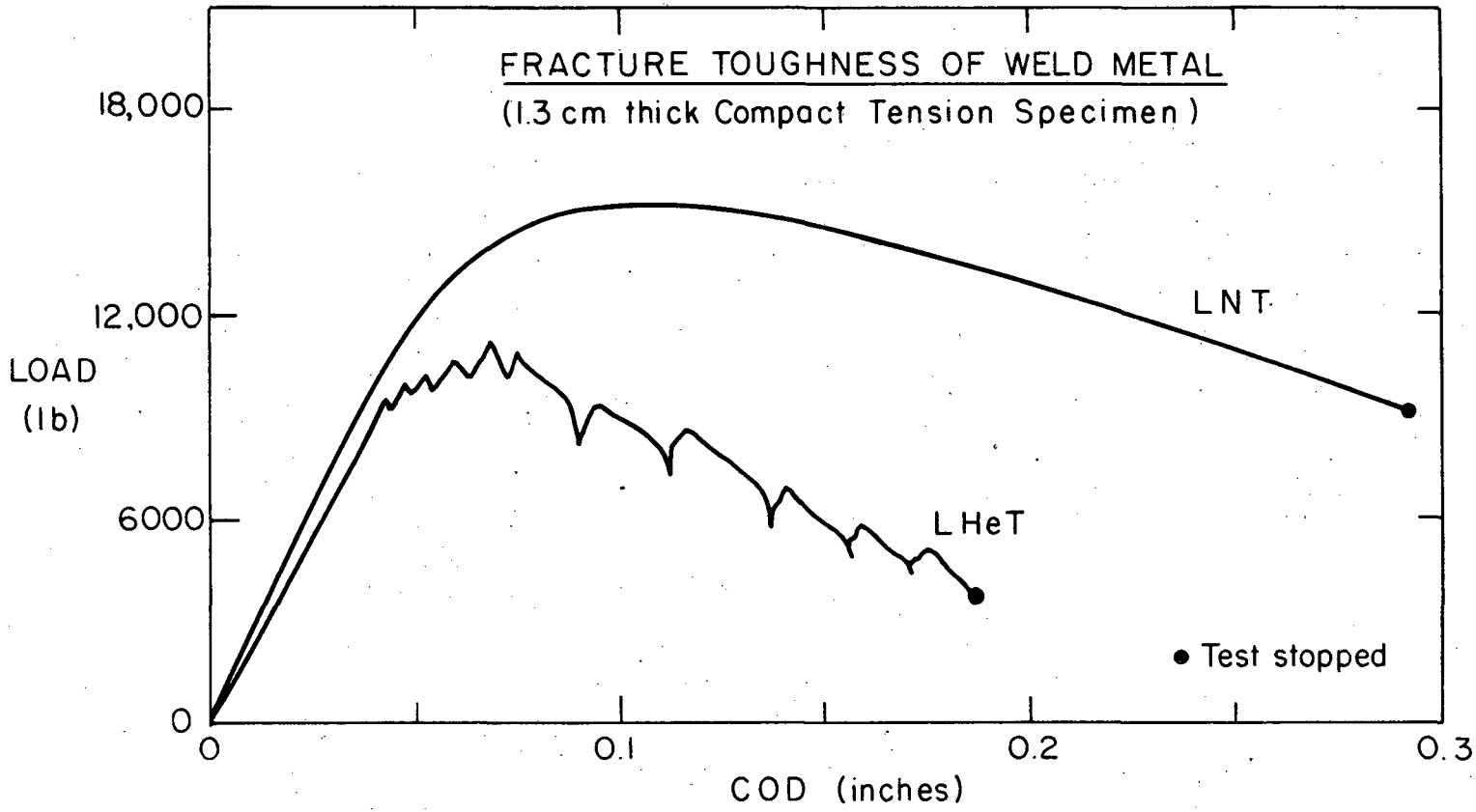

Figure 16

XBL 816-5854

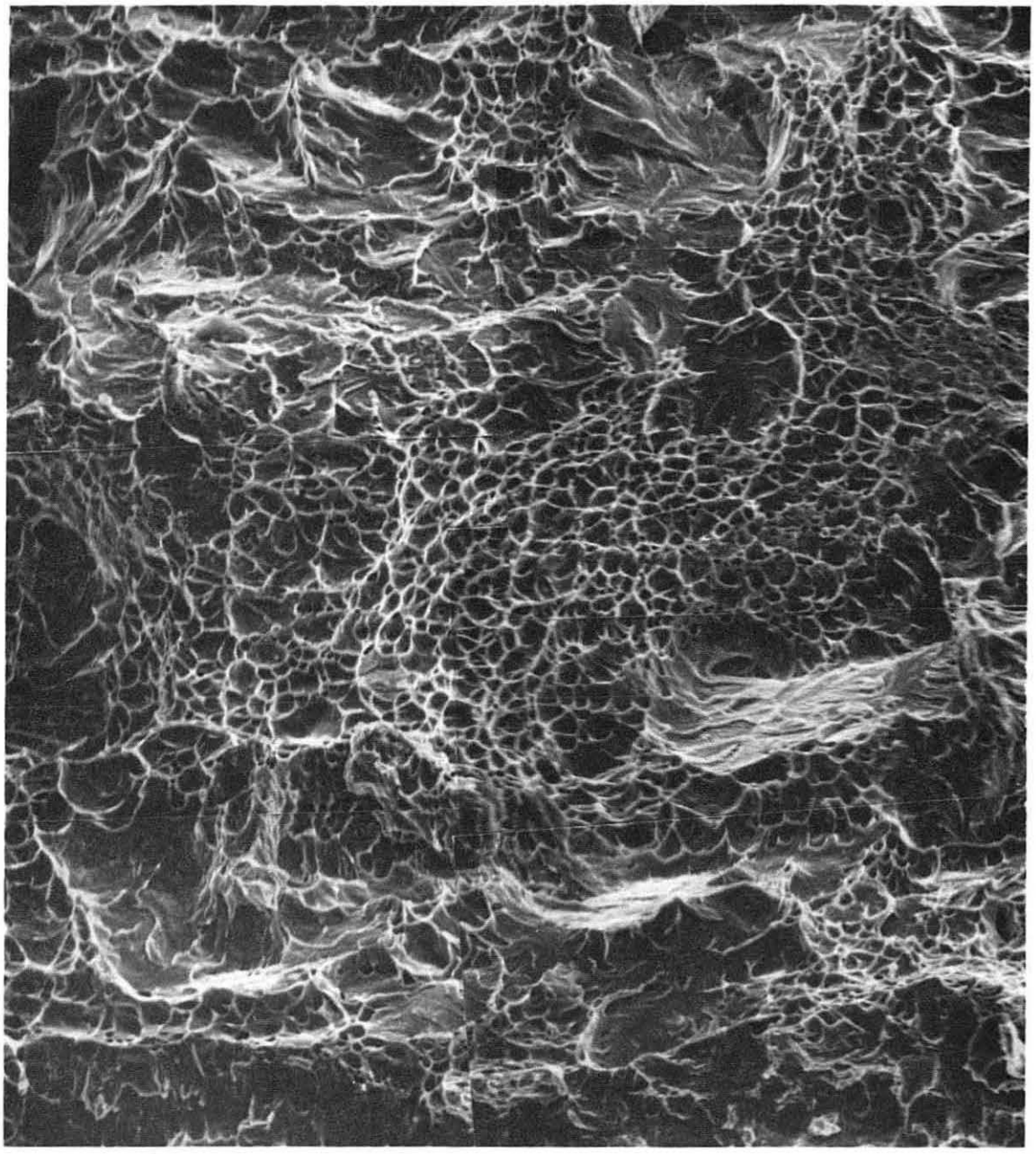

XBB 800-11400

Figure 16

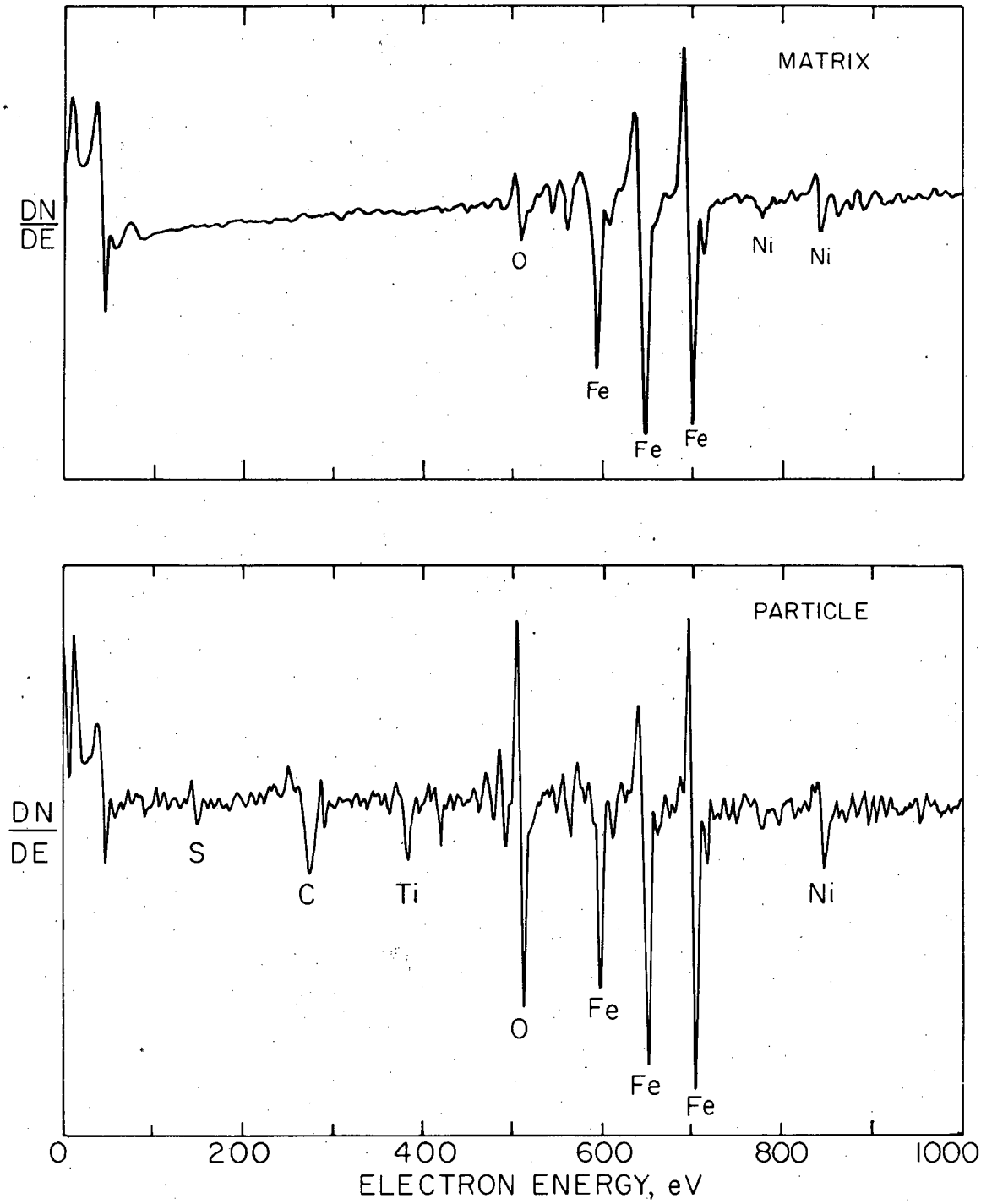

Figure 17

XBL 805-5176A

This report was done with support from the Department of Energy. Any conclusions or opinions expressed in this report represent solely those of the author(s) and not necessarily those of The Regents of the University of California, the Lawrence Berkeley Laboratory or the Department of Energy.

Reference to a company or product name does not imply approval or recommendation of the product by the University of California or the U.S. Department of Energy to the exclusion of others that may be suitable.

TECHNICAL INFORMATION DEPARTMENT
LAWRENCE BERKELEY LABORATORY
UNIVERSITY OF CALIFORNIA
BERKELEY, CALIFORNIA 94720